ELSEVIER

International Journal of Heat and Fluid Flow 19 (1998) 393–400

International Journal of HEAT AND FLUID FLOW

Computation of flow and heat transfer through rotating ribbed passages

Hector Iacovides [1]

Department of Mechanical Engineering, UMIST, P.O. Box 88, Manchester, M60 1QD, UK

Abstract

This study focuses on the computation of periodic flow and heat transfer through stationary and rotating ducts of square cross-section, with rib-roughened walls. Square-sectioned ribs, normal to the flow direction are employed along two opposite walls. Flow comparisons are presented for a duct under stationary and rotating conditions, with ribs in a staggered arrangement. The rib-height-to-diameter ratio is 0.1 and the rib-pitch-to-rib-height ratio is 10. Heat transfer comparisons are shown for a stationary duct with in-line ribs. The rib-height-to-diameter ratio is 0.0675 and the rib-pitch-to-rib-height ratio is 10. Body-fitted grids are employed and two zonal models of turbulence are tested; a k–ϵ with the 1-equation model of k transport across the near-wall regions and a low-Re version of the basic DSM model, in which in the near-wall region the dissipation rate, ϵ, is obtained from the wall distance. The numerical approach adopted leads to the efficient calculation of flows through ribbed ducts. Both models yield satisfactory mean flow predictions and the DSM is also able to reproduce most of the features of the turbulence field, under both stationary and rotating conditions. Though the computations of the coefficient of wall heat transfer are not as close to the data as the flow predictions, the DSM thermal computations are clearly superior to those of the k–ϵ/1-equation.

Notation

c	turbulence modelling constants
D	duct diameter
e	rib height
f	damping functions
h	coefficient of wall heat transfer ($\equiv hDq_w/T_w - T_B$)
k	turbulent kinetic energy
ℓ	turbulent length scale
Nu	Nusselt number ($\equiv hD/\lambda$)
P	mean pressure or rib spacing
P_{ij}	generation rate of u_iu_j
P_k	generation rate of turbulence
Pr	molecular Prandtl number
q_w	wall heat flux per unit area
Re	mean flow Reynolds number ($\equiv h\mathrm{D}W_BD/\nu$)
Ro	dimensionless rotation number ($\equiv h\mathrm{D}\Omega D/W_B$)
T	mean temperature
T_B	fluid bulk temperature
T_W	wall temperature
t	fluctuating temperature
U_i	mean velocity vector
u_i	fluctuating velocity vector
$\overline{u_iu_j}$	turbulent stress tensor
V	cross-duct velocity
W	streamwise velocity
W_B	bulk velocity
X_i	distance from centre of rotation
Y	wall distance or cross-duct co-ordinate direction
y^*	dimensionless wall distance ($\equiv Yk^{1/2}/\nu$)
Z	streamwise direction

Greek

δ	Kronecker delta
ϵ_{ijk}	unit third order tensor
ϵ	dissipation rate of turbulence
λ	thermal conductivity
μ	dynamic viscosity
ν	kinematic viscosity
ρ	density
σ	turbulent Prandtl number
Φ_{ij}	redistribution term
Ω_j	rotation vector

1. Introduction

As can be seen in numerous experimental studies, such as Han (1984), the introduction of rib-roughness can considerably enhance wall heat transfer. Hence, heat-transfer-enhancing ribs are often employed in blade cooling and also in other cooling applications. In the case of blade cooling, such ribs are employed along the surfaces of internal passages within rotating blades and nozzle-guide vanes. As intended, the presence of surface ribs leads to flow separation, on either side of each rib, and to a general rise in turbulence and heat transfer levels. The presence of the rib, as can be seen in the measurements of

[1] E-mail: h.iacovides@umist.ac.uk.

0142-727X/98/$ – see front matter
PII: S0142-727X(98)10023-1

Humphrey and Whitelaw (1979), also induces or reinforces stress-gradient-difference secondary flow. The secondary flow found in the asymmetrically ribbed duct investigated by Humphrey and Whitelaw as not, however, the rotational motion found in square ducts with smooth walls (Melling and Whitelaw, 1976; Gessner and Jones, 1965).

The blade rotation, which is about an axis normal to the direction of the coolant flow, produces a Coriolis force normal to the main flow direction. As shown in Fig. 1(a), in flows through rectangular passages the Coriolis force generates secondary motion across the passage (Moon, 1964). The Coriolis force also directly influences the turbulence field, raising the turbulence levels along the pressure (trailing) side of the rotating passage. In two-dimensional flows through rotating channels (Johnston et al., 1972) only the direct Coriolis effects on turbulence are present, while in three-dimensional flows through rotating rectangular ducts, the Coriolis-driven secondary motion is expected to exert the major influence. The resulting flow is consequently three-dimensional, highly turbulent and, as shown in earlier studies of smooth rotating passages (Iacovides and Launder, 1991, 1995; Bo et al., 1995a) influenced by secondary motion that is stronger along the near-wall regions. Experimental studies (Wagner et al., 1989), have revealed that rotation also influences wall heat transfer in rotating passages, enhancing heat transfer along the pressure side and suppressing it over the suction (leading) side. In blade cooling passages, consequently, the thermal behaviour would be influenced by the presence of secondary motion, rib-induced separation and also by the effects of the Coriolis force on turbulence. As far as the computation of such flows is concerned, the implication is that the turbulence model employed needs to be able to cope with the presence of curvature- and Coriolis-driven secondary motion, the presence of flow separation and also be sensitive to the effects of the Coriolis force on turbulence. Moreover, the elliptic nature of such flows requires the use of fine three-dimensional grids and, as recent studies suggest (Bo et al., 1995a, b), use of high order schemes for the discretization of convective transport.

As shown in earlier studies (Choi et al., 1989; Besserman and Tanrikut, 1991), the resolution of the secondary motion requires the integration of the mean flow equations across the wall sub-layer, making the wall function approach inappropriate. Subsequent work on flows through rotating ducts (Bo et al., 1995b) and through U-ducts of strong curvature, Iacovides et al. (1996), revealed that use of low-Re second-moment closures further improves predictions of flows affected by orthogonal rotation and also by the combined presence of secondary motion and flow separation.

Similarly, extensive numerical studies of the flow and thermal development in rotating ribbed ducts have not, until recently, been possible because of the understandable absence of detailed experimental data. Though some numerical studies of three-dimensional flows through ribbed passages have appeared (Taylor et al., 1991), most have been confined to two-dimensional flows, like Liou et al. (1993). Recent experimental work at University of Manchester Institute of Science and Technology, UMIST (Iacovides et al., 1996) has produced detailed LDA measurements for flow through rotating ducts with ribbed surfaces, thus providing the necessary validation data for the present study.

This study has been confined to the computation of flows through passages that are long enough for repeating flow conditions to prevail over each rib interval. Consequently, flow through only one rib-interval has been examined, using periodic flow boundary conditions. The objective has been to apply effective-viscosity and also simple second-moment closures to the computation of flow and heat transfer through such passages, in order to assess their effectiveness.

2. Flow equations

All equations are expressed here in Cartesian tensor notation, for a rotating frame of reference.

2.1. Mean motion

Continuity

$$\frac{\partial}{\partial x_i}(\rho U_i) = 0.$$

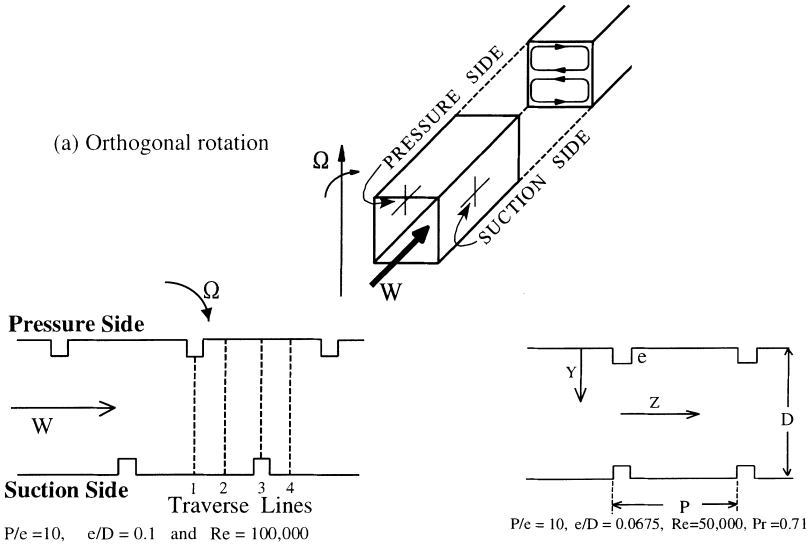

(b) Square duct with staggered ribs (c) Square duct with in-line ribs

Fig. 1. Flow geometries and conditions.

Momentum transport

$$\frac{\partial}{\partial x_j}(\rho U_i U_j) = -\frac{\partial P}{\partial x_i} + \frac{\partial}{\partial x_j}\left[\mu\left(\frac{\partial U_i}{\partial x_j} + \frac{\partial U_j}{\partial x_i}\right) - \rho\overline{u_i u_j}\right] - 2\rho\epsilon_{ijp}\Omega_p U_j - \rho\left[\Omega_j X_j \Omega_i - \Omega_j X_i \Omega_j\right].$$

Enthalpy

$$\frac{\partial}{\partial x_i}(\rho U_j T) = \frac{\partial}{\partial x_i}\left|\frac{\mu}{\mathrm{Pr}}\frac{\partial T}{\partial x_i} - \rho\overline{u_j t}\right|.$$

2.2. Turbulent flow equations

The earlier studies, discussed in Section 1, suggest that a low-Reynolds-number model of turbulence needs to be employed across the near-wall regions and that the use of second-moment closures is also desirable. In order to reconcile these requirements with the need for grid economy, two zonal models have been selected; the high-Re version of the k–ϵ matched to a low-Re 1-equation model of k transport and a simple version of the stress transport model, arising from a low-Re ASM closure employed in earlier computations of flow and heat transfer through smooth rotating ducts (Bo et al., 1995a, b), in which across the near-wall regions the dissipation rate of turbulence is obtained from the wall distance. These models have also been recently applied with reasonable success to the computation of heat transfer in two-dimensional ribbed passages, Iacovides and Raisee (1997).

Effective viscosity model (EVM), Jones and Launder (1972):

$$\rho\overline{u_i u_j} = \frac{2}{3}k\delta_{ij} - \mu_t\left(\frac{\partial U_i}{\partial x_j} + \frac{\partial U_j}{\partial x_i}\right), \mu_t = \rho c_\mu \frac{k^2}{\epsilon},$$

$$\frac{\partial}{\partial x_j}(\rho U_j k) = \frac{\partial}{\partial x_j}\left[\left(\mu + \frac{\mu_t}{\sigma_k}\right)\frac{\partial k}{\partial x_j}\right] + P_k - \rho\epsilon,$$

$$P_k = -\rho\overline{u_i u_j}\left(\frac{\partial U_i}{\partial x_j}\right),$$

$$\frac{\partial}{\partial x_j}(\rho U_j \epsilon) = \frac{\partial}{\partial x_j}\left[\left(\mu + \frac{\mu_t}{\sigma_\epsilon}\right)\frac{\partial \epsilon}{\partial x_j}\right] + c_{\epsilon 1}\frac{\epsilon}{k}P_k - \rho c_{\epsilon 2}\frac{\epsilon^2}{k}.$$

Across the near-wall regions (Wolfshtein, 1969):

$$\epsilon = \frac{k^{3/2}}{\ell_\epsilon}, \quad \mu_t = \rho c_\mu \ell_\mu \sqrt{k}.$$

The length scales ℓ_ϵ and ℓ_μ are obtained from the near-wall distance Y, according to

$$\ell_\epsilon = 2.55Y[1 - \exp(-0.263y^*)],$$
$$l_\mu = 2.55Y[1 - \exp(-0.016y^*)],$$

where $y^* = Yk^{1/2}/v$ is the dimensionless wall distance.

Low-Re differential stress model (DSM), Iacovides and Toumpanakis (1993):

$$\frac{\partial}{\partial x_k}\left(\rho U_k \overline{u_i u_j}\right) = \frac{\partial}{\partial x_k}\left[\left(\mu + \frac{\mu_t}{\sigma_k}\right)\frac{\partial \overline{u_i u_j}}{\partial x_k}\right] + P_{ij} - \rho\epsilon_{ij} + \Phi_{ij} - \left[H_{ij} - \frac{1}{3}H_{kk}\delta_{ij}\right] + J_{ij},$$

$$P_{ij} = -\left[\overline{u_i u_k}\frac{\partial U_j}{\partial x_k} + \overline{u_j u_k}\frac{\partial U_i}{\partial x_k}\right] - 2\Omega_p\left(\epsilon_{ipq}\overline{u_q u_j} + \epsilon_{jpq}\overline{u_q u_i}\right),$$

$$\phi_{ij} = -c_1\frac{\epsilon}{k}\left(\overline{u_i u_j} - \frac{2}{3}k\delta_{ij}\right) - c_2\left(P_{ij} - \frac{2}{3}P_k\delta_{ij}\right) + f_w\left(\phi^w_{ij1} + \phi^w_{ij2}\right),$$

$$\epsilon_{ij} = \frac{2}{3}(1 - f_\epsilon)\epsilon\delta_{ij} + f_\epsilon\frac{\overline{u_i u_k}}{k}\epsilon.$$

The conventional wall reflection terms are used, which rely on the wall distance x_n and the unit vector normal to the wall n:

$$\phi^w_{ij,2} = c^w_2\frac{\epsilon}{k}\left(\phi_{km2}n_k n_m\delta_{ij} - \frac{3}{2}\phi_{ik2}n_k n_j - \frac{3}{2}\phi_{jk2}n_k n_i\right)\left\{\frac{k^{1.5}}{\epsilon c_\ell x_n}\right\},$$

$$\phi^w_{ij,1} = c^w_1\frac{\epsilon}{k}\left(\overline{u_k u_m}n_k n_m\delta_{ij} - \frac{3}{2}\overline{u_k u_i}n_k n_j - \frac{3}{2}\overline{u_k u_j}n_k n_i\right)\left\{\frac{k^{1.5}}{\epsilon c_\ell x_n}\right\},$$

$$\phi_{ij2} = -c_2\left(P_{ij} - \frac{2}{3}P_k\delta_{ij}\right).$$

The low-Re terms H_{ij} and J_{ij} are defined as

$$H_{ij} = f_H\frac{v}{k}\left(\overline{u_i u_\ell}\frac{\partial\sqrt{k}}{\partial x_\ell}\frac{\partial\sqrt{k}}{\partial x_j} + \overline{u_j u_\ell}\frac{\partial\sqrt{k}}{\partial x_\ell}\frac{\partial\sqrt{k}}{\partial x_i}\right),$$

$$J_{ij} = f_J k\left(\frac{\partial U_i}{\partial x_j} + \frac{\partial U_j}{\partial x_i}\right)$$

The damping functions that appear in the above terms have the following expressions:

$$f_\epsilon = \exp(-y^*/3), \quad f_w = [1 - \exp(-0.12y^*)][1 + \exp(-0.03y^*)],$$

$$f_J = 0.06\ \exp(-y^*/3),$$
$$f_H = (10.2 + 7.5y^*)\ \exp(-y^*/20).$$

The dissipation rate equation is identical to that used in the EVM model. In the near-wall regions, the dissipation rate, ϵ, is also obtained from a prescribed length scale ℓ_ϵ, obtained from

$$\ell_\epsilon = 2.55Y[1 - \exp(-0.236y^*)].$$

Turbulent heat fluxes: The same approximation has been employed for both stress models, namely the effective diffusivity approximation.

$$\rho\overline{u_i t} = -\frac{\mu_t}{\sigma_T}\frac{\partial T}{\partial x_i}.$$

In earlier work involving the computation of flow and heat transfer through two-dimensional ribbed passages, Iacovides and Raisee (1997), the generalised gradient hypothesis was also used for the modelling of the turbulent heat fluxes in the DSM computations. This alternative approximation to the turbulent heat fluxes did not, however result in any noticeable predictive improvements.

The empirical constants that appear in the turbulence equations have the following values, according to the proposals of Jones and Launder (1972) for the k and ϵ equations and Gibson and Launder (1978) for the stress equations:

c_μ	$c_{\epsilon 1}$	$c_{\epsilon 2}$	c_1	c_2	c^w_1	c^w_2	σ_k	σ_ϵ	σ_T
0.09	1.44	1.92	1.8	0.6	0.5	0.3	1	1.3	0.9

3. Cases computed

Flow computations through two types of ribbed passages have been obtained, both of square cross-section; a passage with staggered square ribs along two opposite walls, Fig. 1(b) and a passage with in-line square ribs along opposite walls, Fig. 1(c). For the former type, flow computations have been obtained with the passage either stationary, or orthogonally rotating about an axis parallel to the ribs and comparisons

have been carried out with the LDA data of Iacovides et al., 1996. For the latter type, heat transfer computations have also been obtained, using air ($Pr = 0.7$) as the working fluid and comparisons have been carried out with Nusselt number measurements of Baughn and Yan (1992).

4. Numerical aspects

A three-dimensional non-orthogonal finite volume solver, STREAM, was employed, developed at UMIST, which solves for the Cartesian velocity components. A collocated grid is employed with mass flux modification to prevent pressure chequerboarding. In the case of the DSM model, use of the apparent viscosity concept prevents numerical oscillations arising from the explicit presence of the Reynolds stress gradients in the momentum transport equations. For the discretization of convective transport, a bounded form of the quadratic upstream interpolation scheme (QUICK) by Leonard (1979) is employed in the solution of all transport equations, details of which are provided by Iacovides (1997).

In the heat transfer computations, constant wall heat flux thermal boundary conditions were employed. The repeating flow boundary conditions are imposed by first applying a bulk velocity correction at the exit plane, so as to maintain the specified flow rate, and then setting the entry conditions the same as those at the exit plane. For the temperature field, the temperature distribution at the entry plane is set equal to that at the exit plane, but with a bulk adjustment which maintains a constant temperature at a reference point, within the entry plane.

In order to minimise the number of grid nodes required, body-fitted grids, shown in Fig. 2, have been employed. This approach, allows for a more efficient distribution of the grid nodes and a more effective resolution of the near-wall regions. Both grids shown in Fig. 2, consisted of $76 \times 64 \times 30$ nodes, along the streamwise direction, between the ribbed walls and between the symmetry plane and the smooth wall respectively.

For the duct with staggered ribs, a coarser $38 \times 32 \times 15$ mesh was also used, shown in Fig. 3, for grid sensitivity comparisons. Comparisons of the resulting EVM predictions along the symmetry plane, traverse lines 1 and 2, for the stationary case, are shown in Fig. 4. The mean velocity profiles obtained with the two grids are practically identical and are also in close agreement with the LDA data. These comparisons provide some support for the numerical and griding strategy adopted. [2]

5. Results and discussion

5.1. Flow in a square duct with staggered ribs

Fig. 5 shows the mean flow development along the symmetry plane of a stationary duct. The separation bubble downstream of each rib extends to almost half the inter-rib distance. Profile comparisons along traverse lines 1 and 2 of the duct symmetry plane, are presented in Fig. 6. Iacovides et al. (1996) state that the uncertainties in the measured mean velocities and turbulence intensities were within 2% of the mean velocity. As already commented, the EVM computed velocity profiles are in close agreement with the measurements. The DSM comparisons return a somewhat faster core flow,

[2] More recent tests have further revealed that heat transfer computations obtained with an intermediate grid, with half the number of grid nodes of the fine mesh, produced heat transfer predictions identical to those of the fine mesh.

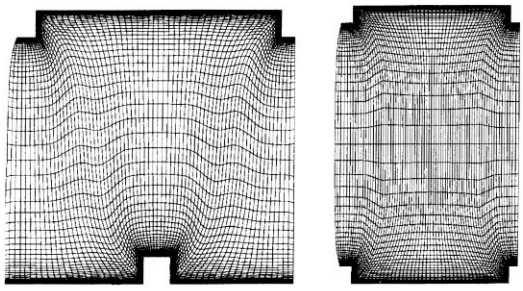

(a) Staggered Ribs (b) In-line Ribs

Fig. 2. Body-fitted grids employed, $76 \times 64 \times 30$ nodes.

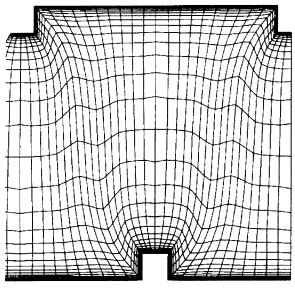

Fig. 3. Coarse mesh employed for grid sensitivity comparisons. $38 \times 32 \times 15$ nodes.

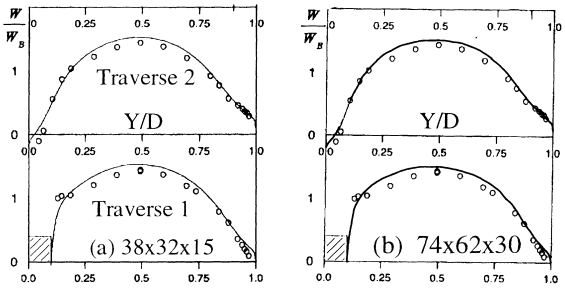

Fig. 4. EVM computations of the streamwise velocity for a stationary passage with staggered ribs.

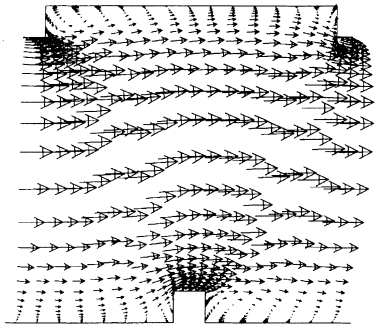

Fig. 5. Mean flow along the symmetry plane, for a stationary duct.

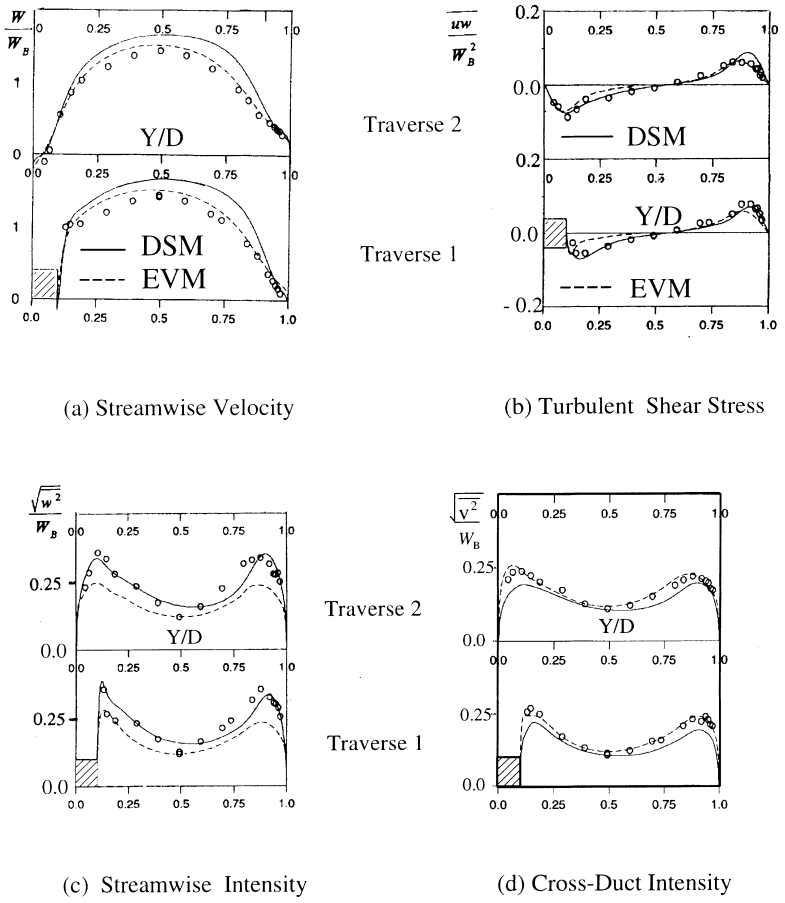

Fig. 6. Profile comparisons for stationary passage with staggered ribs.

which appears to be consistent with the fact, shown later in Fig. 11, that the DSM model returns a significant turbulence-driven secondary motion. The comparisons of the stress profiles show that both models reproduce the high turbulence levels measured. The DSM model tested is also found able to reproduce the levels of the individual stresses, in the streamwise and cross-duct directions, with reasonable accuracy, the maximum difference for either component being less than 10%. The experimental distribution of the turbulent shear stress is also well reproduced, especially by the DSM model, with measured and predicted levels being practically identical. The corresponding EVM predictions are also not far from the LDA data. As far as the turbulence intensities are concerned, the trends present in the measurements are reproduced, but the levels of streamwise intensities are in places under-predicted by as much as 30%. Shear stress levels over the rib are severely under-predicted by the EVM model, by as much as 50%.

For the rotating case at a rotation number ($\mathrm{Ro} \equiv \Omega D/W_B$) of 0.2, the mean flow development along the symmetry plane is shown in Fig. 7. The size of the flow separation regions along the pressure (trailing) side is reduced, while along the suction side the separation bubbles are enlarged. Mean-velocity profile comparisons along the symmetry-plane traverse lines 1–4 are shown in Fig. 8. The mean flow measurements indicate that the Coriolis-induced secondary motion convects the faster fluid toward the pressure (trailing) side of the duct. The mean velocity field is well reproduced by both models. Moreover, because the Coriolis-driven secondary motion is a mean flow phenomenon, differences between the DSM and EVM predictions have diminished.

The corresponding stress comparisons are shown in Fig. 9. As expected, rotation raises the levels of all measured components of the Reynolds stress tensor along the pressure side of the duct. Some of this rise in the pressure-side turbulence levels is reproduced even by the EVM model, indicating that it is partly caused by the Coriolis-driven secondary motion. The DSM model produces a stronger variation in the levels of the normal stresses across the duct and the computed distribution of the streamwise component is in good accord with the data. The cross-duct component is somewhat under-predicted

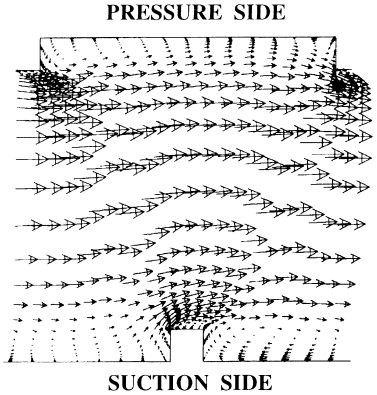

Fig. 7. Mean flow along the symmetry plane, for a rotating duct, at $\mathrm{Ro} = 0.2$.

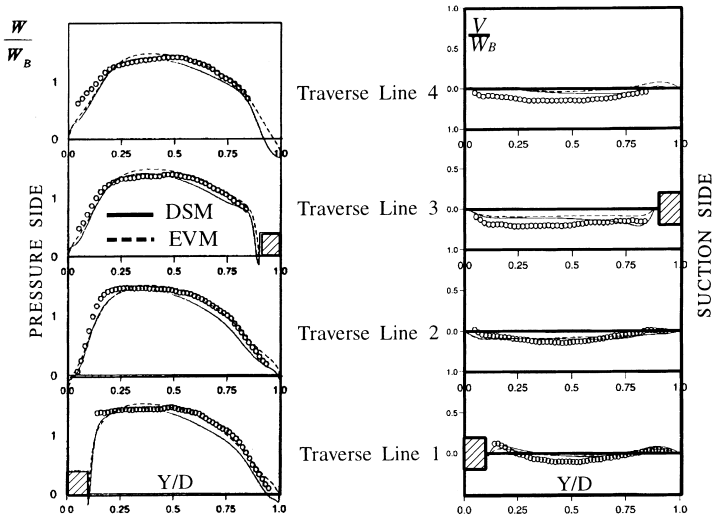

(a) Streamwise Velocity (b) Cross-Duct Velocity

Fig. 8. Mean flow comparisons for rotating passage with staggered ribs, at Ro = 0.2.

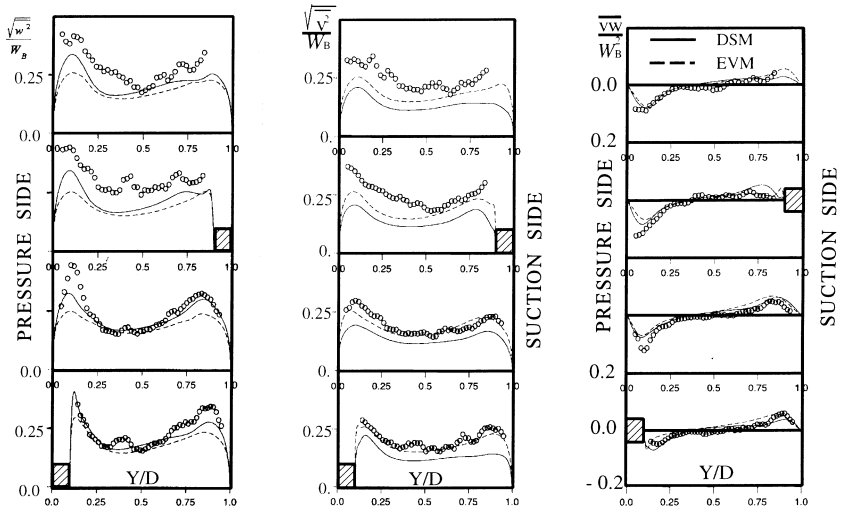

(a) Streamwise Intensity (b) Cross-Duct Intensity (c) Shear Stress

Fig. 9. Turbulence field comparisons for rotating passage with staggered ribs, at Ro = 0.2.

by the DSM model, while both models return shear stress levels comparable to those measured. The DSM model returns a shear stress distribution that is in closer overall agreement with the measurements than that of the EVM model.

On the whole, the main effects of rotation on the turbulence field are reproduced by the DSM model employed, but agreement with measurements is not as close as in the stationary case.

5.2. Heat transfer in a square duct with in-line ribs

The flow development for this case is shown in the symmetry-plane vector plots of Fig. 10, where the separation bubbles on either side of each rib are clearly visible. The cross-duct vector plots of Fig. 11, at a plane half-way between the ribs, show that, as commented earlier, the DSM model produces a turbu-

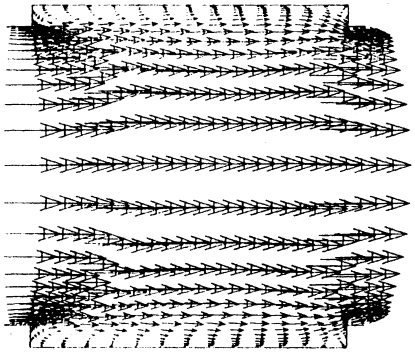

Fig. 10. Mean flow along symmetry plane of square duct with in-line ribs.

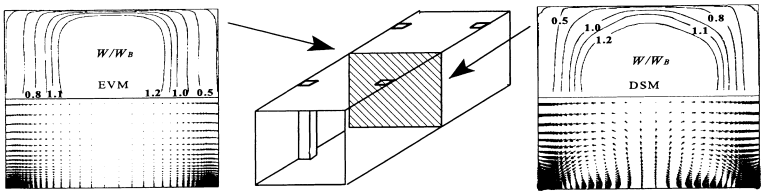

Fig. 11. Predicted flow field across the duct, half-way between the in-line ribs.

lence-driven secondary motion that influences the distribution of the streamwise velocity. The secondary motion returned by the DSM for this symmetrically ribbed duct is, however, more similar to that measured in ducts with smooth walls, Melling and Whitelaw (1976), than to that measured in asymmetrically ribbed ducts by Humphrey and Whitelaw (1979).

Comparisons between the computed and measured distributions of the local Nusselt number, along the centre line of the ribbed wall, are shown in Fig. 12. Baughn and Yan (1992), estimated that the Nusselt number was measured with an uncertainty of 6.4%. Both the level and distribution of the local Nusselt number are better reproduced by the second-moment closure, though there is still scope for further improvement. The stronger secondary motion returned by the DSM must be at least partly responsible for the higher Nusselt number levels returned by this model, which in places are still as much as 20% lower than the experimental ones. It is especially noteworthy that over the rib, while the EVM model under-predicts the high Nusselt number values measured, the DSM values are close to the experimental levels. This is consistent with the earlier finding that over the rib, the EVM model also under-predicts the turbulent shear stress.

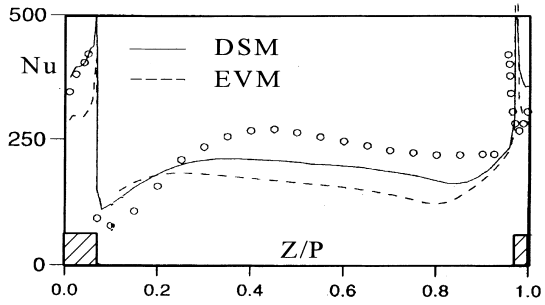

Fig. 12. Local Nusselt number comparisons along the centre line of the ribbed wall of a passage with in-line ribs.

Comparisons between the predicted contours of the local Nusselt number along the ribbed wall and those measured by Baughn and Yan (1992), shown in Fig. 13, also show that the DSM model reproduces the experimental distribution more faithfully, over the entire ribbed wall. The EVM model returns a faster recovery downstream of the rib, which is at variance with the data and also fails to return the dip found in the corner region, upstream of the rib.

As also shown in Fig. 12, near the symmetry plane, both models and, especially, the EVM, show a gradual rise in Nusselt number levels ahead of the rib, not present in the data.

The heat transfer comparisons thus reveal that the models tested are less successful in reproducing the thermal behaviour than they are in returning the flow development in ribbed ducts. The comparisons also reveal that there are important differences between the thermal predictions of the DSM and the EVM models, suggesting that a second-moment closure produces predictive improvements.

6. Concluding remarks

From the comparisons carried out, a number of conclusions can be drawn regarding the computation of flow and heat transfer through ribbed and rotating passages.

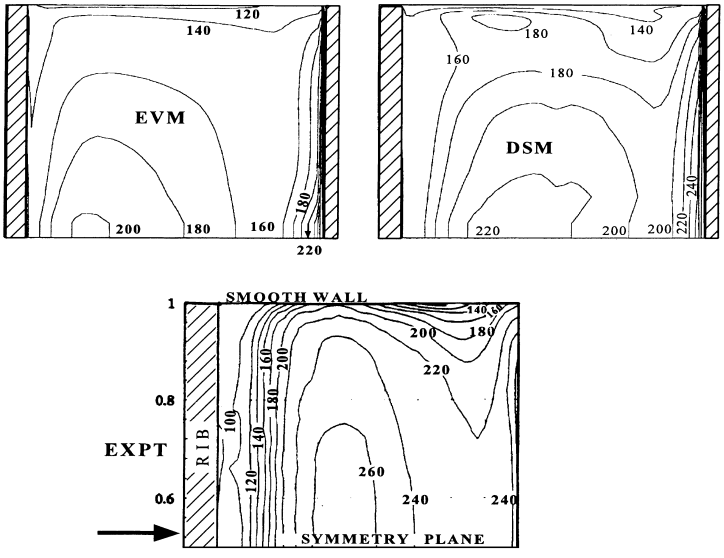

Fig. 13. Contours of the local Nusselt number, along the ribbed wall, for a square duct with in-line ribs.

The use of body-fitted grids and high-order discretization schemes for the convective transport leads to the efficient resolution of flow through ribbed ducts.

The mean flow development in *stationary* ribbed ducts is well predicted by the zonal k–ϵ/1-equation model, while the rather simple low-Re DSM employed somewhat over-predicts the strength of the turbulence-driven secondary motion. Both models return the high turbulence levels measured, and the DSM model also returns satisfactory predictions of the anisotropy of turbulence and, in contrast to the EVM model, predicts the correct shear stress levels over the ribs.

In ribbed ducts *rotating orthogonally*, both the above models reproduce well the mean flow development. The effects of rotation on turbulence are well reproduced by the DSM model, but agreement with the measurements is not as close as in the stationary case.

The *thermal behaviour* in ribbed ducts, is not well predicted by the k–ϵ/1-equation model. Introduction of a simple low-Re DSM, in which the near-wall dissipation rate is obtained from the wall distance, improves thermal predictions, because of its ability to predict the turbulence-driven secondary motion and also because it is able to return the correct turbulence field over the ribs. More refined turbulence models are however necessary to achieve the close agreement with the experimental data, observed in the hydrodynamic comparisons.

Acknowledgements

The author wishes to express his gratitude to his colleague Prof. B.E. Launder for his support and encouragement. Support for this work has been provided by Rolls-Royce plc and DRA Pyestock. The helpful input of Mr J. Coupland, of Rolls-Royce plc is gratefully acknowledged. Thanks are also due to Dr. Y.-M. Yuan at UMIST for making available the experimental data in digital form.

References

Baughn, J.W., Yan, X., 1992. Local heat transfer measurements in square ducts with transverse ribs. ASME National Heat Transfer Conference.

Besserman, D.L., Tanrikut, S., 1991. Comparison of heat transfer measurements with computations for turbulent flow around a 180° bend. ASME Paper 91-GT-2, International Gas-Turbine and Aero Congress. Orlando FL.

Bo, T., Iacovides, H., Launder, B.E., 1995a. Developing buoyancy-modified turbulent flow in ducts rotating in orthogonal mode. ASME Journal of Turbomachinery 117, 474–484.

Bo, T., Iacovides, H., Launder, B.E., 1995b. Convective discretization schemes for the turbulence transport equations in flow predictions through sharp U-bends. International Journal of Numerical Methods in Heat and Fluid Flow 5, 33–48.

Choi, Y.-D., Iacovides, H., Launder, B.E., 1989. Numerical computation of turbulent flow in a square-sectioned 180-deg bend. ASME Journal of Fluids Engineering 111, 59–68.

Gressner, F.B., Jones, J.B., 1965. On some aspects of fully-developed turbulent flow in rectangular channels. JFM 23, 689.

Gibson, M.M., Launder, B.E., 1978. Ground effects on pressure fluid fluctuations in atmospheric boundary layers. JFM 86, 491.

Han, J.C., 1984. Heat transfer and friction characteristics in channels with two opposite rib-roughened walls. ASME Journal of Heat Transfer 106, 774–781.

Humphrey, J.A.C., Whitelaw, J.H., 1979. Turbulent flow in ducts with roughness. In: Second International Symposium on Turbulent Shear Flows. London.

Iacovides, H., 1997. The computation of turbulent flow through stationary and rotating u-bends of with rib-roughened surfaces. In: 11th International Conference on Laminar and Turbulent Flows. Swansea.

Iacovides, H., Launder, B.E., 1991. Parametric and numerical study of fully-developed flow and heat transfer in rotating rectangular ducts. ASME Journal of Turbomachinery 113, 331.

Iacovides, H., Launder, B.E., 1995. Computational fluid dynamics applied to internal cooling of gas-turbine blade cooling: A review. International Journal of Heat and Fluid Flow 16, 454–470.

Iacovides, H., Raisee, M., 1997. The computation of flow and heat transfer in two-dimensional rib-roughened passages. In: Second International Symposium on Turbulence Heat and Mass Transfer. Delft.

Iacovides, H., Toumpanakis, 1993. Turbulence modelling of flow in axisymmetric rotor-stator systems. In: Proceedings of IAHR, Fifth International Symposium on Refined flow modelling and Turbulence Measurements. Paris.

Iacovides, H., Jackson, D.C., Ji, H., Kelemenis, G., Launder, B.E., Nikas, K., 1996. LDA study of flow development through an orthogonally rotating U-Bend of strong curvature and rib-roughened walls. Paper No ASME-96-GT-476, International Gas-Turb and Aero Congress. Birmingham, UK.

Johnston, J.P., Halleen, R.M., Lezius, D.K., 1972. Effects of spanwise rotation on the structure of two-dimensional fully developed turbulent channel flow. JFM 56, 533–557.

Jones, W.P., Launder, B.E., 1972. The prediction of laminarization with a two-equation model of turbulence. International Journal of Heat Mass Transfer 15, 301–314.

Leonard, B.P., 1979. A stable and accurate convective modelling procedure, based on quadratic interpolation. Computational Methods in Applied Mechanics and Engineering 19, 59–68.

Liou, T.M., Hwang, J.J., Chen, S.H., 1993. Simulation and measurement of enhanced turbulent heat transfer, in a channel with periodic ribs on one principal wall. International Journal of Heat Mass Transfer 36, 507–517.

Melling, A., Whitelaw, J.H., 1976. Turbulent flow in a rectangular duct. JFM 78, 289.

Moon, I.M., 1964. Effects of Coriolis force on turbulent boundary layers in rotating fluid machines. MIT Gas-Turbine Laboratory, Report No. 74.

Taylor, C., Xia, J.Y., Medwell, J.O., Morris, W.D., 1991. Numerical simulation of three-dimensional turbulent flow and heat transfer within a multi-rib cylindrical duct. ASME Paper 91-GT-8, International Gas Turbine and Aero Engines Congress.

Wagner, J.H., Johnson, B.V., Hajek, T.J., 1989, Heat transfer in rotating passages with smooth walls. ASME, Paper 89-GT-272, International Gas-Turbine and Aero Engines Congress.

Wolfshtein, M., 1969. The velocity and temperature distribution in one-dimensional flow with turbulence augmentation and pressure gradient. International Journal of Heat and Mass Transfer 12, 301.